Materials Advances

ROYAL SOCIETY OF CHEMISTRY

PAPER

View Article Online
View Journal | View Issue

Cite this: *Mater. Adv.*, 2025, 6, 2691

A new and facile preparation of 3D urchin-like TiO_2@graphene core@shell SERS substrates for photocatalytic degradation of RhB†

Nguyen Thi Huyen,[ab] Tran Ai Suong Suong,[c] Cao Thi Thanh,[a] Pham Van Trinh,[a] Nguyen Van Tu,[a] Bui Hung Thang,[a] Tran Van Hau,[a] Pham Thanh Binh,[a] Vu Duc Chinh,[a] Pham Van Hai,[de] Vu Xuan Hoa,[f] Tran Van Tan,[g] Phan Ngoc Minh,[b] Hiroya Abe[h] and Nguyen Van Chuc *[ab]

Received 16th January 2025,
Accepted 23rd March 2025

DOI: 10.1039/d5ma00040h

rsc.li/materials-advances

Here, we present a new and facile method to grow a graphene (Gr) shell layer on the surface of a 3D urchin-like TiO_2 core layer (TiO_2@Gr) on a silicon (Si/SiO_2) substrate as a surface enhanced Raman scattering (SERS) substrate for detecting and degrading rhodamine B (RhB) under UV irradiation. The core layer of 3D urchin-like TiO_2 (UT) was fabricated by a hydrothermal method and a Gr shell layer was grown on the surface of the TiO_2 core layer by a thermal chemical vapor deposition (CVD) method with sodium deoxycholate (SDC) surfactant as a carbon source. The obtained results indicated that the minimum detectable concentration of RhB on the TiO_2@Gr/SERS substrate-coated graphene (UTG) can reach 1×10^{-9} M with an enhancement factor (EF) of 1.3×10^5. The enhancement of the Raman signals of the UTG can be generated because the graphene acts as the electron acceptor of TiO_2 and prevents charge recombination, and provides indirect charge transfer from TiO_2 to RhB molecules. The UTG SERS substrate can almost completely decompose RhB with a degradation rate of 0.069 min^{-1} under UV irradiation at 254 nm within 80 min. The photocatalytic degradation mechanism of UTGs towards RhB was also presented in detail. The results show that the UTG SERS substrate can be further employed for detecting substances and degrading hazardous pollutants.

1. Introduction

To measure the degree and rate of organic contaminant degradation at low levels, a number of analytical approaches have been developed to monitor the photo-degradation process, including UV-Vis spectrophotometry,[1] gas chromatography-mass spectrometry (GC-MS),[2] and high-performance liquid chromatography (HPLC).[3] However, UV-Vis spectrophotometry can detect only the concentration of molecules without detecting the chemical structure of the molecules during the degradation of organic contaminants and the intermediates during the photocatalytic process. Compared to UV-Vis, GC-MS and HPLC measurements can be used to identify the intermediates of molecules. Nevertheless, these measurements are still restricted due to quite complicated, costly testing equipment, and are time-consuming.[4] Therefore, it is necessary to develop an *in situ* method to detect the chemical structure of molecules and identify the intermediates during the photocatalytic degradation process of organic contaminants. Recently, the surface-enhanced Raman scattering (SERS) technique has emerged as a powerful tool for detecting and analyzing the structure of chemical and biological molecules due to its high sensitivity, short analysis times, non-destructive determination, easy sample preparation, and lack of requirement for sample extraction and separation.[5,6]

Among semiconductor materials, titanium dioxide (TiO_2) has been extensively used in the photodegradation of environmental pollutants due to its high photocatalytic activity,

[a] *Institute of Materials Science, Vietnam Academy of Science and Technology, 18 Hoang Quoc Viet, Cau Giay, Hanoi, Vietnam. E-mail: chucnv@ims.vast.vn*
[b] *Graduate University of Science and Technology, Vietnam Academy of Science and Technology, 18 Hoang Quoc Viet, Cau Giay, Hanoi, Vietnam*
[c] *VNU University of Engineering and Technology, 144 Xuan Thuy, Cau Giay, Hanoi, Vietnam*
[d] *Faculty of Physics, Hanoi National University of Education, 136 Xuan Thuy, Cau Giay, Hanoi, Vietnam*
[e] *Institute of Natural Sciences, Hanoi National University of Education, 136 Xuan Thuy, Cau Giay, Hanoi, Vietnam*
[f] *Institute of Science and Technology, TNU-University of Sciences (TNUS), Tan Thinh ward, Thai Nguyen City, Vietnam*
[g] *Faculty of Physics, University of Science, Vietnam National University, Hanoi, 334 Nguyen Trai, Thanh Xuan, Hanoi, Vietnam*
[h] *Joining and Welding Research Institute, Osaka University, Osaka 5670047, Japan*
† Electronic supplementary information (ESI) available. See DOI: https://doi.org/10.1039/d5ma00040h

stability, and nontoxicity.[7–11] However, TiO_2 has weak SERS signals for detecting chemical and biological molecules.[6,7,12] To improve the SERS signals and photocatalytic activity of the TiO_2 material, it is necessary to develop new methods for producing TiO_2 and TiO_2 composite materials with different sizes, shapes, and crystal structures. Compared to zero dimensional (0D), one dimensional (1D) and two dimensional (2D) structures, three dimensional (3D) structures of TiO_2 have advantages such as high surface area-to-volume ratio, low aggregation, and easy separation of particles from solution. Hence, the 3D TiO_2 can provide more space for adsorbing analyte molecules and permit the diffusion of analyte molecules into the structure, and thus will enhance surface reactions.[13] Moreover, to enhance the SERS signals and the photocatalytic degradation, TiO_2 has been combined with nanostructured noble metals (Ag, Au) and/or carbon nanomaterials (graphene, carbon nanotubes).[6–10] With high charge carrier mobility, mechanical flexibility, large surface area, and high absorption of organic molecules through π–π interactions, graphene (Gr) is a good candidate for applications in surface-enhanced Raman scattering (SERS)[10,14–16] and photocatalytic degradation.[9,11] Due to its unique optoelectronic and electronic properties, the TiO_2-Gr hybrid material has emerged as a star material for providing effective charge transfer (CT) between analyte molecules and the substrate surface and electron transport in photocatalysis.[7,10] The TiO_2-Gr hybrid material has been used to enhance both SERS signals and photocatalytic degradation of environmental pollutants, such as rhodamine 6G,[9] rhodamine B,[17] and tetracycline medicine.[17]

The TiO_2-Gr hybrid material can be fabricated by some methods, such as thermal chemical vapor deposition (CVD),[18–21] solvo/hydrothermal,[22–24] sol–gel,[25] and mechanical mixing.[26,27] Among these above methods, only the thermal CVD method can synthesize TiO_2-Gr hybrid materials with a Gr layer covered TiO_2 core to form a TiO_2@Gr core–shell structure. Some previous studies have used carbon sources such as methane gas (CH_4),[18,21] acetylene gas (C_2H_2),[20] propylene gas (C_3H_6), and methanol (CH_3OH)[19] for the fabrication of TiO_2@Gr core–shell structure hybrid materials. However, most previous reports have only focused on synthesizing graphene layers directly onto the surface of TiO_2 nanoparticles[19,20] or flat TiO_2 substrates.[18,21] To the best of our knowledge, a 3D urchin-like TiO_2@Gr core–shell structure hybrid material synthesized by thermal CVD and used as a SERS substrate to enhance the Raman signal and photocatalytic degradation of rhodamine B has not been reported yet.

In the present study, 3D urchin-like TiO_2 (UT) on a silicon (Si/SiO_2) substrate was fabricated by a hydrothermal method and a Gr shell layer was grown on the surface of the TiO_2 core by the thermal CVD method with sodium deoxycholate (SDC) surfactant as a carbon source. The fabricated 3D urchin-like TiO_2@Gr core–shell (UTG) samples were used as SERS substrates to detect and decompose rhodamine B (RhB) under UV irradiation. Furthermore, a possible charge transfer mechanism for the SERS enhancement effect and photocatalytic degradation mechanism for UTG towards RhB were also presented in detail.

2. Experimental

2.1. Materials

Titan tetrachloride ($TiCl_4$, 99%), hydrochloric acid (HCl, 37%), absolute ethanol (C_2H_5OH, 99.7%), rhodamine B (RhB, 99%), ethylenediaminetetraacetic acid disodium (EDTA, 99%), isopropyl alcohol (IPA, > 99%), and benzoquinone (BQ, 99%) were purchased from Macklin Co. Ltd (China). Gases such as hydrogen (H_2, >99%), argon (Ar, >99%) were purchased from Messer Co. Ltd (Hai Phong, Vietnam). Sodium deoxycholate (SDC, 96%) was purchased from Fujifilm Co. Ltd (Japan).

2.2. Fabrication of 3D urchin-like TiO_2

The 3D urchin-like TiO_2 (UT) was grown on a silicon substrate (Si/SiO_2) by a hydrothermal method. Firstly, 10 mL HCl was added into 10 mL deionized water, and then 0.3 mL $TiCl_4$ was added under stirring for 20 min at 7–10 °C. The obtained solution was put into a stainless-steel autoclave of 50 mL volume, followed by placing the Si/SiO_2 substrates (0.5 cm × 0.5 cm) horizontally on the floor of the autoclave. Then, the autoclave was kept at 160 °C for 6 h and then naturally cooled to room temperature. After that, the as-prepared samples were washed with deionized water and ethanol, dried at 50 °C for 30 min and annealed at 400 °C for 1 h in air, and UT samples were obtained.

2.3. Fabrication of a 3D urchin-like TiO_2@Gr core–shell

The 3D urchin-like TiO_2@Gr (UTG) core–shell was fabricated by the thermal chemical vapor deposition (CVD) method with SDC surfactant as a carbon source for the growth of a graphene (Gr) shell layer. Briefly, a mixed solution of 25 μL SDC solution and ethanol with a ratio of 3 : 1 was dropped onto the surface of the TiO_2 samples. Afterwards, the samples were dried for 24 h at room temperature. Before the CVD process for growing a graphene layer, the reactor quartz tube and all gas lines were purged in Ar gas flow of 300 standard cubic centimeter (sccm) for 30 min. Then, the TiO_2 samples covered with SDC were inserted into a quartz tube and heated at 800 °C with a heating rate of 10 °C min^{-1} in a mixture of Ar (50 sccm) and H_2 (30 sccm) gases for 30 min. After the CVD process, the H_2 gas was shut off and the samples were cooled down naturally to room temperature in Ar gas flow.

2.4. Characterizations

The surface morphologies of the samples were measured by field emission scanning electron microscopy (FESEM, Hitachi S-4800, Japan) at an accelerating voltage of 5 kV, and transmission electron microscopy (TEM, JEM 2100, Joel, Japan) at an accelerating voltage of 200 kV. The crystal structures of samples were determined by X-ray diffraction (XRD, D8 Advance, Bruker, Germany) with Cu-Kα radiation (λ = 1.5406 Å) at 40 kV and 20 mA over the 2-theta range of 10°–80°. The energy dispersive X-ray spectrum (EDS) mapping of the samples was determined by SEM (JSM-IT800, Joel, Japan). Photoluminescence (PL) spectra were done by using a spectrofluorometer (FL3-22 JobinYvon Spex, USA).

2.5. SERS and photodegradation measurements

SERS and photodegradation properties of UT and UTG core–shell samples were investigated through detecting the Raman vibrational signals of the RhB molecule. 20 μL of RhB solutions with various concentrations (10^{-1}–10^{-9} M) were uniformly drop coated onto the surface of the samples. The photodegradation performances of the RhB molecules on the samples under ultraviolet light (UV) radiation (UV lamp source with parameters: power (66 W), wavelength (254 nm), length (45 cm), and diameter (2.5 cm)), manufactured by Medicor, Budapest, Hungary, type (BLF-12) were measured at room temperature by a Raman spectrophotometer (LabRAM HR Evolution, Horiba, Japan) using an objective lens of 100× with a 532 nm excitation source. In UV light irradiation, the UT and UTG core–shell samples on the Si/SiO_2 substrates were placed below a UV lamp source with a distance of 5 cm. Procedures of preparation and RhB degradation of 3D urchin-like TiO_2@graphene SERS substrates under irradiation of UV light are displayed in Scheme 1. The adsorption and photocatalytic activities of the samples were also measured *via* UV-visible absorption spectrophotometer (UV-2450, UV/Vis spectrophotometer, Shimadzu, Japan).

3. Results and discussion

3.1. The morphology, structure and composition characterization of 3D urchin-like TiO_2@Gr core–shell

The morphology, size and microstructure of 3D urchin-like TiO_2 (UT) and 3D urchin-like TiO_2@graphene (UTG) core–shell were observed by SEM and TEM images, as shown in Fig. 1a–d. It is observed that UTs are covered by numerous nanoneedles, which grow radially from the core of the microspheres and grow uniformly on the surface of the Si/SiO_2 substrate. The diameter range of the UTs is from 10 μm to 12 μm, as shown in Fig. 1a. The thickness of the UT layer covered on the surface of the Si/SiO_2 substrate is about 65 μm (Fig. 1b). Fig. 1c and d are high-magnification SEM images of UTs and UTGs, respectively. Fig. 1c and d indicate that the surface of the UT and UTG microspheres is very smooth and clean. The HRTEM image in the inset of Fig. 1c shows that the distance between the adjacent lattice fringes of the UT crystals is about 0.32 nm. This distance is attributed to the interplanar distance of rutile TiO_2 (110).[18,28–30] The nanoneedles are grown along the rutile (110) crystal plane, and with a preferred orientation in the [001] direction.[29,30]

The hydrothermal reactions of the growth of the rutile TiO_2 nanoneedles were as follows:[31,32]

$$TiCl_4 + H_2O \rightarrow HCl + Ti_{(IV)}\ \text{complex} \quad (1)$$

$$Ti_{(IV)}\ \text{complex} \xrightarrow{\text{dehydration}} TiO_2 \quad (2)$$

The presence of abundant amounts of Ti^{4+} precursor, H^+, and Cl^- ions contributes to the formation of rutile TiO_2. The presence of highly acidic conditions may reduce the hydrolysis of the Ti source, and the selective adsorption of Cl^- on rutile

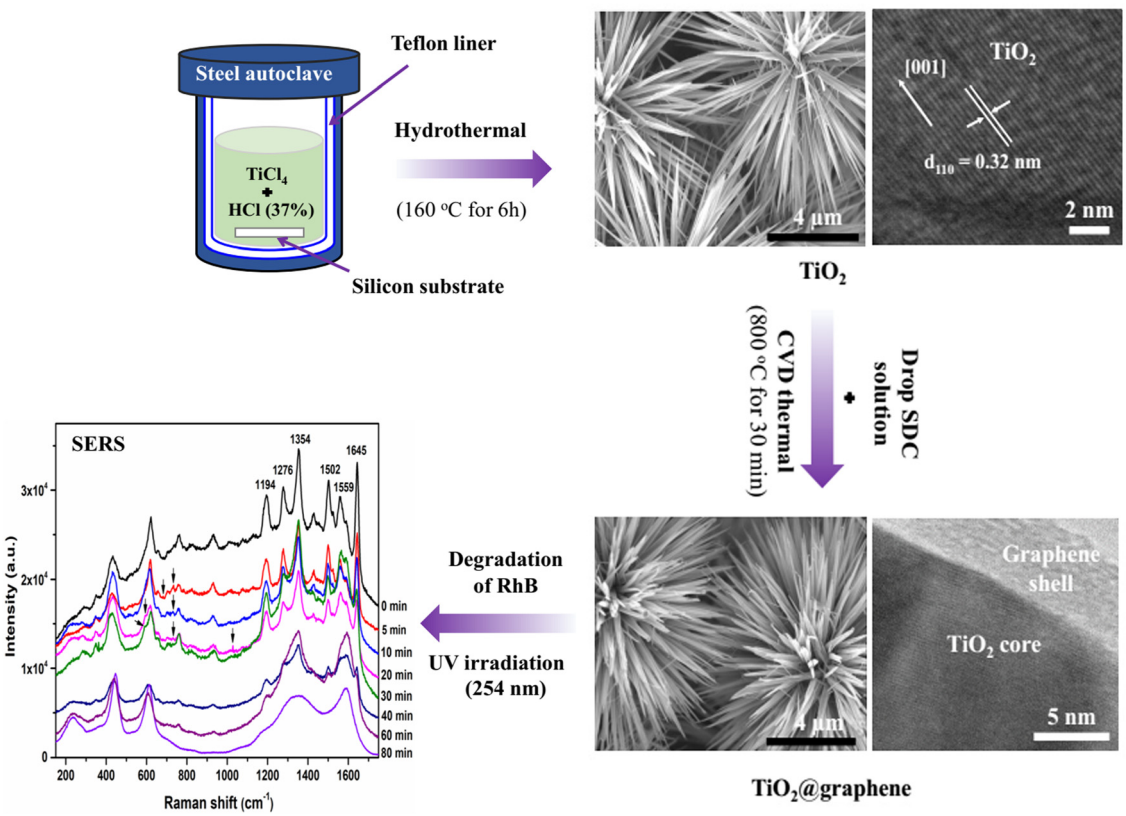

Scheme 1 Fabrication procedure and RhB degradation of TiO_2@graphene SERS substrates under the irradiation of UV light.

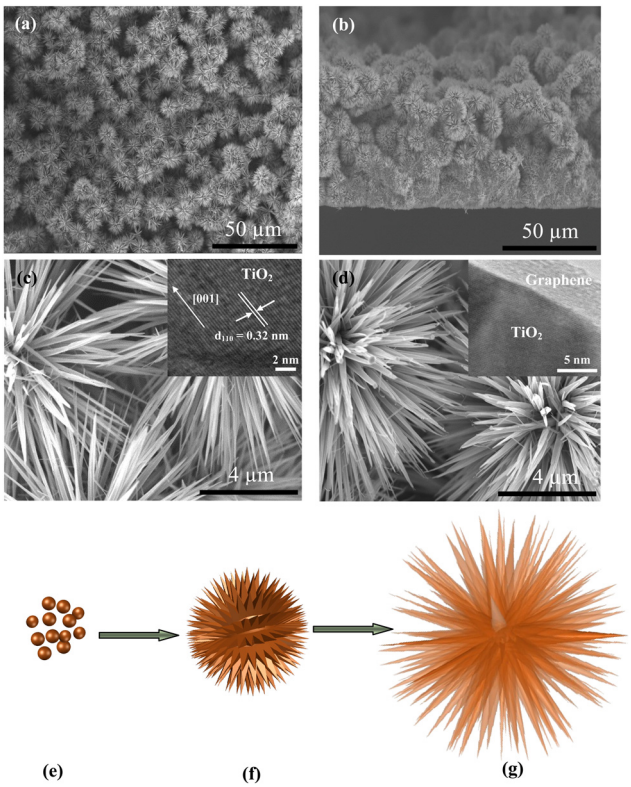

Fig. 1 Surface and cross sectional SEM images (a) and (b) of UTs on the SiO_2 substrate, high-magnification SEM images and the insets are HRTEM images of (c) UTs and (d) UTGs. Schematic illustration of the formation process of the UTs: (e) nucleation, (f) dissolution and recrystallization, and (g) self-assembly.

(110) can promote the anisotropic growth along the [001] direction of rutile TiO_2.[31,32]

As reported previously,[29,30] the mechanism that is responsible for the formation of the 3D urchin-like TiO_2 (UT) structure may follow a process of nucleation, dissolution and recrystallization, and self-assembly, as shown in Fig. 1e–g. At the first stage, amorphous or rutile nuclei of TiO_2 were formed, and then they coalesced into crinkly spherical units as shown in Fig. 1e. These TiO_2 spherical units dissolved and recrystallized to gradually form TiO_2 nanoneedles on the surface of the microspheres (Fig. 1f). Finally, the 3D urchin-like TiO_2 structures were formed due to the directional self-assembly of the TiO_2 nanoneedles (Fig. 1g).

The thickness of graphitic layer covered TiO_2 was provided from the HRTEM image. As shown in the HRTEM image in the inset of Fig. 1d, a very thin layer graphitic structure was observed on the surface of the UT. The thickness of the graphitic layer was about several nm. Furthermore, the presence of graphitic layer covered TiO_2 was confirmed by the energy dispersive X-ray spectroscopy (EDS) elemental mapping (Fig. 2). The EDS results (Fig. 2a) show that the UTG was composed of Ti, O and C elements without other elements, and the corresponding contents are 49.6 wt%, 46.2 wt% and 4.1 wt%, respectively. Fig. 2b and c suggests that the Ti (orange), O (green), and C (red) elements were uniformly distributed in the UTGs.

Fig. 3a and b show XRD patterns and Raman spectra of the UT and UTG samples, respectively. As shown in Fig. 3a, the prepared UT exhibits main diffraction peaks at $2\theta = 27.5^\circ$, 36.1°, 39.2°, 41.3°, 44.1°, 54.4°, 56.7°, 62.8°, and 64.1° corresponding to the (1 1 0), (1 0 1), (200), (111), (2 1 0), (2 1 1), (2 2 0), (002), and (310) planes of TiO_2 rutile (JCPDS no. 01-087-0710).[28] The peaks are sharp and intense, indicating good crystallinity of TiO_2. For UTG, the XRD pattern also shows the main diffraction peaks of TiO_2 crystals with rutile phase. However, the diffraction peaks of graphitic carbon cannot be detected in the XRD patterns (Fig. 3a). This is possibly due to the small amount of graphitic carbon grown onto the surface of UT and/or due to the strong diffraction of rutile TiO_2.

Fig. 3b presents the Raman spectra of the UT and UTG samples. As shown in Fig. 3b, the prepared UT shows the presence of three peaks at 607 cm^{-1}, 442 cm^{-1}, and 235 cm^{-1} corresponding to the rutile phase.[33] The Raman spectrum of the UTG sample after growth of graphitic carbon also shows three rutile peaks of TiO_2 and three important graphitic bands at ~1330 cm^{-1}, ~1600 cm^{-1}, and ~2630–2640 cm^{-1}

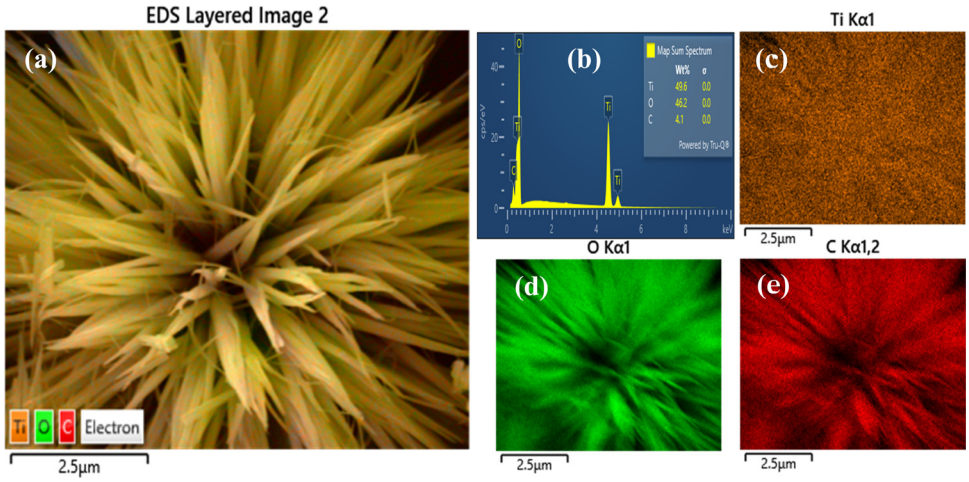

Fig. 2 (a) SEM image, (b) EDS spectrum, and (c)–(e) elemental mapping images of (c) Ti, (d) O and (e) C elements of UTG.

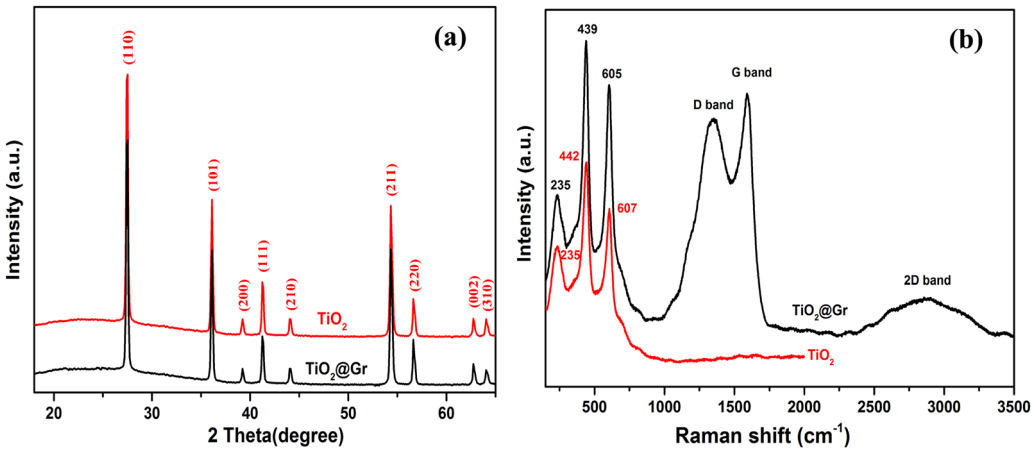

Fig. 3 (a) XRD and (b) Raman spectra of UT and UTG samples.

corresponding to the D band, G band, and 2D band, respectively. The D band and G band are characteristics of structure defects and sp^2-hybridization of carbon atoms, respectively. The 2D band, the second-order Raman of the D band, is the characteristic band corresponding to the number of graphitic sheets that form the multi-layer graphene structure.[18,34–38] These important characteristic peaks of graphitic confirmed the presence of graphene (Gr) structures in the crystalline structure of TiO_2 rutile. Moreover, compared to the Raman spectrum of the UT sample, there is a red-shift of about 2 cm^{-1} for the 605 cm^{-1} band and about 3 cm^{-1} for the 439 cm^{-1} band. These shifts can be assigned to interactions of TiO_2 with Gr during the thermal CVD process.[18]

3.2. Optical characterizations of 3D urchin-like TiO_2@Gr

The optical characteristics of UT and UTG samples were measured by UV-vis absorption and photoluminescence (PL) spectra. Fig. S1a and b (ESI†) illustrate the absorption spectra and optical band gap of the UT and UTG samples, respectively. As shown in Fig. S1a (ESI†), the absorption edges of the UTG display a red-shift compared with UT. These shifts can be assigned to restoration of the π–π conjugation network of the Gr in the hybrid.[39] Moreover, the incorporation of Gr into the TiO_2 system also reduced the energy band gap of the photocatalyst. According to the Tauc equation, the energy band gaps of UT and UTG were calculated to be around 2.84 eV and 2.77 eV, respectively. In order to study the recombination of photo-induced electron–hole pairs, photoluminescence (PL) measurements were conducted. As shown in Fig. S1c (ESI†), the PL intensity of UTG was lower than that of UT. This attenuation is attributed to Gr's exceptional electron transport properties, which effectively suppress recombination of electron–hole pairs, hence enhancing the photocatalytic degradation efficiency of the organic contaminants.[39]

3.3. SERS characterizations of 3D urchin-like TiO_2@Gr

For comparison, the SERS performance of the UT and UTG samples were studied under the same conditions. The Raman spectra of the RhB molecule with a concentration of 10^{-5} M on the UT and UTG samples are shown in Fig. 4. For the SERS

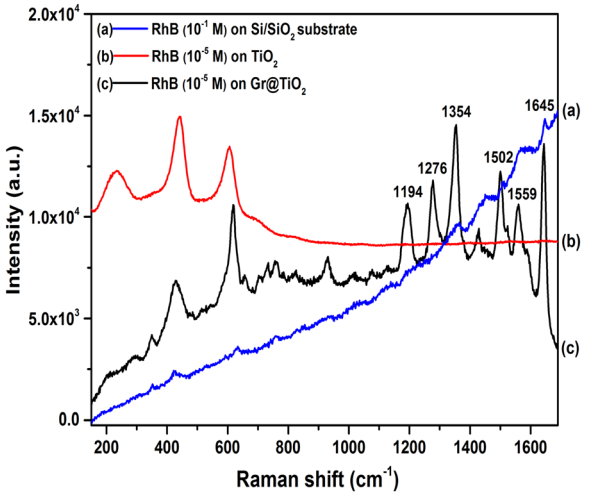

Fig. 4 SERS spectra of RhB adsorbed on: (a) a Si/SiO_2 sample with the concentration of 10^{-1} M, and (b) UT, and (c) UTG samples with an RhB concentration of 10^{-5} M.

substrate of the UT sample, no Raman scattering signals of RhB molecules are detected. For the SERS substrate of the UTG sample, the SERS spectrum shows strong signals of RhB molecules at 1645 cm^{-1}, 1559 cm^{-1}, 1502 cm^{-1}, 1354 cm^{-1}, 1276 cm^{-1}, and 1194 cm^{-1}. The RhB bands at 1645 cm^{-1}, 1559 cm^{-1}, 1502 cm^{-1}, and 1354 cm^{-1} are assigned to aromatic C–C stretching modes;[40] the band at 1276 cm^{-1} is assigned to C–H bending vibration, and the band at 1194 cm^{-1} is attributed to aromatic C–C stretching.[41–43] The SERS properties show the remarkably improved SERS activity of the RhB molecules over the UTG compared to UT. The SERS sensitivity of the UTG substrate can be evaluated by calculating the enhancement factor (EF), using the following equation:[6,44–46]

$$EF = (I_{SERS}/I_{Ref}) \times (C_{Ref}/C_{SERS}) \quad (3)$$

where I_{SERS} and I_{Ref} are the Raman intensities at 1645 cm^{-1} of RhB molecules adsorbed on the TiO_2@Gr/SERS substrates-coated graphene (UTG) and non-SERS substrate (SiO_2). C_{SERS} and C_{Ref} are

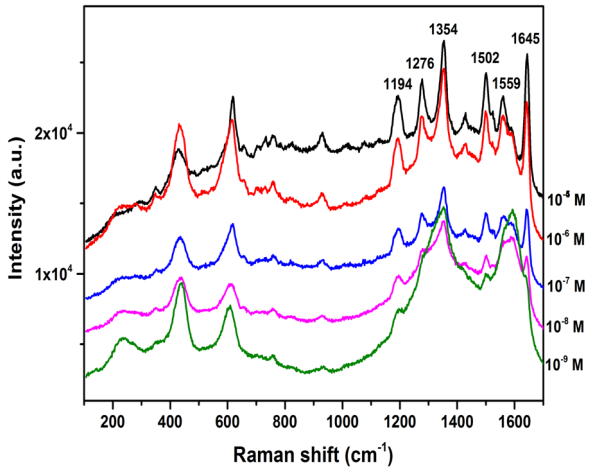

Fig. 5 SERS spectra of RhB adsorbed on UTG samples with the concentration from 10^{-5} M to 10^{-9} M of RhB.

the corresponding concentration of the RhB molecule dropped on the SERS substrate (10^{-5} M) and non-SERS substrate (10^{-1} M). The EF of the UTG SERS substrate calculated for the strongest peak at 1645 cm^{-1} was 1.3 × 10^5 of RhB molecules with a concentration of 10^{-5} M.

Fig. 5 shows the SERS spectra of RhB molecules with concentrations ranging from 10^{-5} M to 10^{-9} M. It can be found that the Raman signal intensities of RhB molecules decrease with decreasing probe molecule concentration and the minimum detection concentration of 10^{-9} M can be detected. The possible charge transfer mechanism for the enhancement effect in the SERS spectra of UTG for the RhB molecules is demonstrated in Fig. 6. The presence of graphene (Gr) in the UTG hybrid structure acts as the electron acceptor and transporter. The excited electrons of TiO_2 can be transferred into Gr from the surface stage energy levels (*E*ss) of TiO_2. The Gr acts as the electron acceptor of TiO_2 and prevents the charge recombination, and provides an indirect charge transfer from TiO_2 to RhB molecules. With excellent conductivity, Gr can promote the transport of charge carriers and the charge transfer efficiency from TiO_2 to RhB molecules. A strong interfacial charge transfer between TiO_2 and Gr would enhance the SERS signals of the RhB molecules.

3.4. Photocatalytic activity of a 3D urchin-like TiO_2@Gr core–shell

The photo-catalytic activity of UTGs was studied by detecting the SERS spectra of RhB molecules. The SERS spectra of the RhB molecules with concentration of 10^{-5} M after the decomposition by UTGs under different UV irradiation times of 0–80 min are shown in Fig. 7a. It can be found that the characteristic Raman peaks of the RhB molecules were gradually decreased with increase of the UV irradiation time. During the degradation process, besides the appearance of the main characteristic Raman peaks of RhB molecules, some strange peaks were also observed at different times, such as 593.8 cm^{-1} (20 min, and 30 min), 732.6 cm^{-1} (5 min, 10 min, and 20 min),

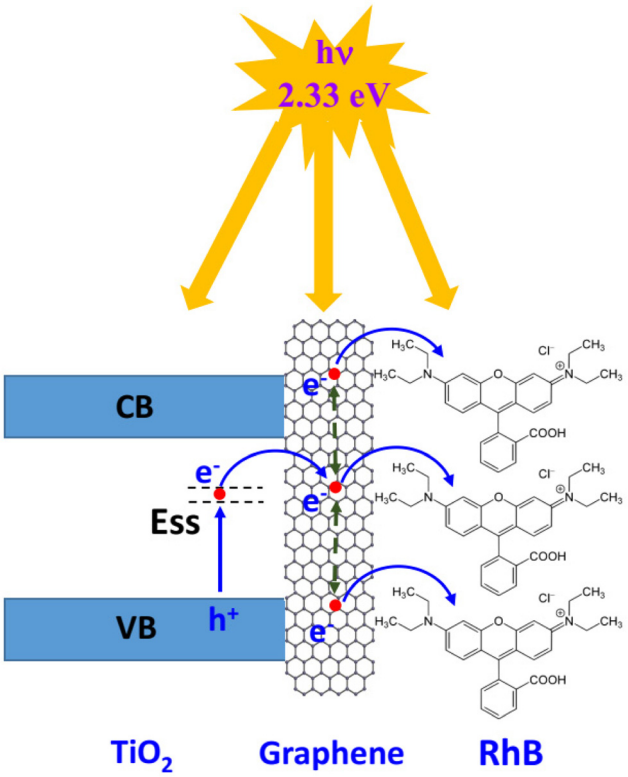

Fig. 6 Possible charge transfer mechanism of TiO_2@graphene/RhB structure.

and 1028.5 cm^{-1} (20 min). These strange peaks could be contributed from the intermediates formed at the interface of the UTGs and air. After the UV irradiation time of 80 min, almost all the peaks of RhB molecules and intermediates had disappeared completely.

The photo-catalytic efficiency of UTs and UTGs was studied through the RhB Raman peak intensity located at 1645 cm^{-1}. This is a peak which has the strongest intensity of RhB in the SERS spectra. The photocatalytic rate (k) was evaluated *via* $ln(P/P_0)$ *versus* the irradiation time (Fig. 7b), where P_0 and P are the intensity of the Raman peaks of RhB initially and after different UV irradiation times, respectively. From the slope of the fitting curve (Fig. 7b), the photocatalytic rate of UTGs is about 0.069 min^{-1}. The photo-catalytic activity of the UTG SERS substrate for RhB degradation under UV irradiation was also compared with previously reported SERS substrates for organic pollutant degradation under different irradiation sources (Table 1).

The photo-catalytic activity of the UTs and UTGs was also studied by UV-visible absorption spectrophotometry (Fig. S2, ESI†). Compared to UV-visible absorption spectrophotometry, the SERS technique can detect the k values of the chemical bonds in the RhB structural changes during the course of RhB degradation at the molecular level, while UV-visible absorption spectrophotometry can detect only the k value of the RhB in the bulk solution. To identify the radical scavengers generated during the photocatalysis reaction, three different capturing agents were introduced into the reaction mixture, namely

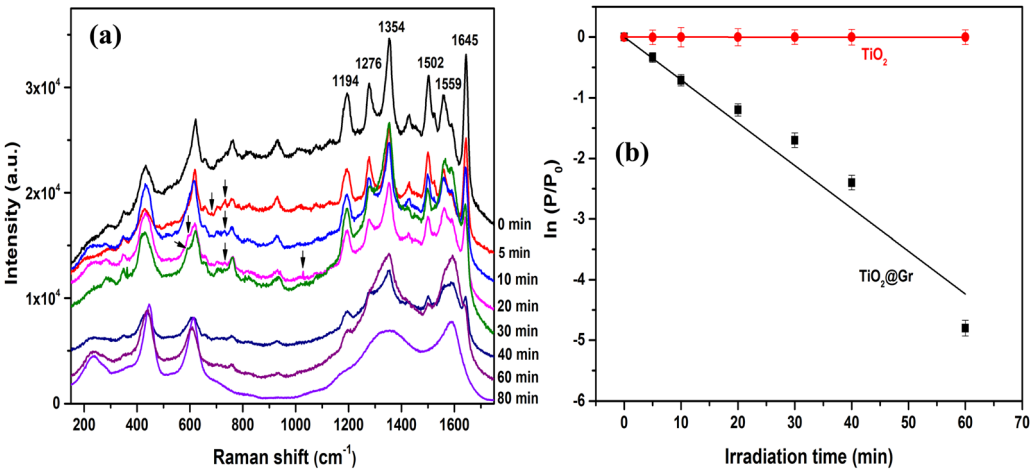

Fig. 7 (a) SERS spectra and (b) linear relation between logarithm of SERS intensities ($\ln(P/P_0)$) at 1645 cm^{-1} *versus* irradiation time (min) for the degradation of RhB.

Table 1 Comparison of photocatalytic activity from different SERS substrates for organic pollutant degradation

SERS substrate for photocatalytic degradation	Probe molecule	Irradiation source	Complete degradation time (min)	Concentration (mol L^{-1})	Degradation rate (k) min^{-1}	Ref.
Ag–G–TiO_2/ G–Ag–TiO_2/ Ag–TiO_2–G	R6G	UV (λ > 410 nm)	60	10^{-6}	0.0371/ 0.0301/ 0.0111	11
Ag/TiO_2 NTs	R6G	UV (254 nm)	140	10^{-6}	0.02479	47
TiO_2/AgNP	R6G	UV (385 nm)	120	10^{-6}	0.029	48
Ag–TiO_2 nanorods	R6G	UV (254 nm)	90	10^{-5}	0.043	49
g-C_3N_4/AuNPs	R6G	Xenon lamp	20	10^{-5}	0.1102	50
Ag–TiO_2 nanotube arrays	R6G	UV (365 nm)	150	10^{-7}	NA	51
ZnO/Ag	RhB	Xenon lamp, 420 nm	150	10^{-5}	NA	43
Ag/PDA/ZnO@GMF	RhB	UV (254 nm)	40	10^{-3}	0.0391	52
Ag/TiO_2	RhB	LED light (370 nm)	120	10^{-3}	NA	53
TiO_2/Ag	RhB	LED light (370 nm)	90	10^{-3}	NA	54
Ag_2CO_3	RhB	Mercury–xenon lamp light	30	10^{-5}	NA	55
CNs/AgNSs@CNQDs-GLs membrane	RhB	Xenon lamp (400 nm)	80	10^{-7}	NA	56
Ag/Cu_2O	RhB	Xenon lamp	120	10^{-7}	NA	57
Ag@SiO_2/CNNDs/EGLs	RhB	Xenon lamp (400 nm)	20	10^{-6}	NA	58
TiO_2@Gr core–shell	RhB	UV (254 nm)	80	10^{-5}	0.069	This work

PDA, polydopamine; glass microfibre filters, GMF; CNs, graphitic–carbon–nitride nanosheets; CNQDs, graphitic–carbon–nitride quantum-dots (CNQDs-GLs); AgNSs, Ag nanospheres; CNNDs, g-C_3N_4 nanodots; EGLs, exfoliated graphene layers.

ethylenediaminetetraacetic acid disodium (EDTA),[59–61] isopropyl alcohol (IPA),[59–63] and benzoquinone (BQ).[59–62] EDTA, IPA, and BQ scavengers were used to trap holes (h^+), hydroxyl radicals ($^\bullet OH$), and superoxide radicals ($^\bullet O_2^-$), respectively. As depicted in Fig. S3 (ESI†), the photocatalytic degradation of RhB by UTGs was found to decrease from 98.5% to 40.2%, 57.3%, and 64.6% in the presence of EDTA, BQ, and IPA, respectively. The k value for the photocatalytic degradation of RhB by UTGs was found to decrease from 0.046 min^{-1} to (0.006–0.014 min^{-1}) in the presence of scavengers under UV light irradiation. The order of inhibition of the photodegradation efficiency was EDTA (h^+) > BQ ($^\bullet O_2^-$) > IPA ($^\bullet OH$). These results suggest that h^+ and $^\bullet O_2^-$ radicals play the main role for the decomposition of RhB, and $^\bullet OH$ plays a relatively minor role in RhB photodecomposition.

The photocatalytic degradation mechanism for UTGs towards RhB is shown in Fig. 8. Under UV light irradiation, the excited electrons from the surface of TiO_2 are transferred from the valence band (VB) of TiO_2 to the conduction band (CB), to thus generate electron–hole (e^-–h^+) pairs (eqn (4)). The photogenerated e^- in the CB of TiO_2 can be transferred to Gr through the intimate interfacial contact between TiO_2 and Gr (eqn(5)). With good conductivity, Gr will enhance the separation and lifetime of the e^-–h^+ pairs and thus will improve the photocatalytic activity of the UTGs. The electrons on the surface of Gr react with dissolved oxygen (O_2) to form radical anions $^\bullet O_2^-$ (eqn (6)). The photogenerated e^- on the TiO_2 surface could also be trapped directly by the O_2 to form radical anions $^\bullet O_2^-$. These radical anions $^\bullet O_2^-$ combine with H_2O molecules to form $^\bullet OH$ radicals (eqn (7)–(9)). Meanwhile, the separated holes are

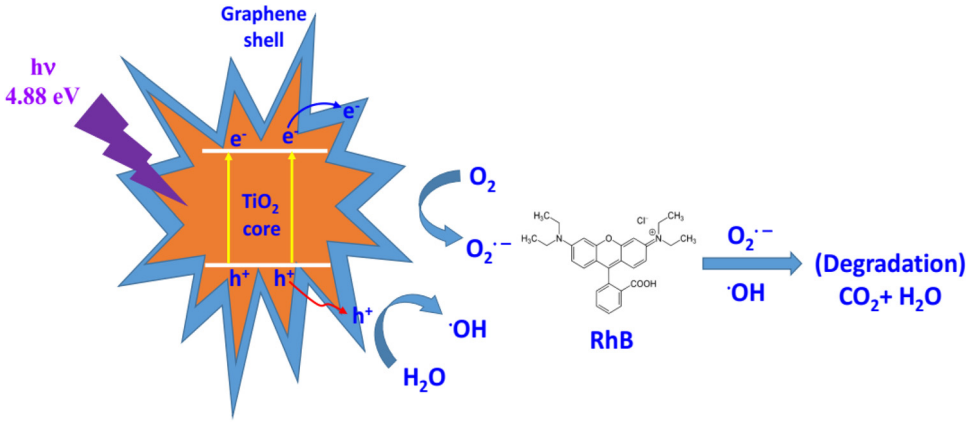

Fig. 8 Degradation mechanism for UTG towards RhB.

consumed to oxidize the dye molecules directly. On the other hand, holes from the VB of TiO_2 can react with either H_2O or OH^- ions adsorbed on the catalyst surface to generate highly reactive $^{\bullet}OH$ radicals (eqn (10)). The holes, $^{\bullet}O_2^-$ and $^{\bullet}OH$ activated radicals degrade RhB molecules into CO_2, H_2O and other intermediates (eqn (11)).[64] The major reaction equations that are involved in the photocatalytic degradation mechanism for UTG towards RhB are described by eqn (4)–(11).

$$TiO_2 + h\nu \rightarrow h^+ + e^- \quad (4)$$

$$TiO_2\ (h^+ + e^-) + \text{graphene} \rightarrow \text{graphene}\ (e^-) + TiO_2\ (h^+) \quad (5)$$

$$\text{Graphene}\ (e^-) + O_2 \rightarrow \text{graphene} + {}^{\bullet}O_2^- \quad (6)$$

$${}^{\bullet}O_2^- + H_2O \rightarrow HO_2{}^{\bullet} + OH^- \quad (7)$$

$$HO_2{}^{\bullet} + H_2O \rightarrow H_2O_2 + {}^{\bullet}OH \quad (8)$$

$$H_2O_2 \rightarrow 2\ {}^{\bullet}OH \quad (9)$$

$$h^+ + OH^- \rightarrow {}^{\bullet}OH \quad (10)$$

$$RhB + h^+/{}^{\bullet}O_2^-/{}^{\bullet}OH \rightarrow CO_2 + H_2O + \text{intermediates} \quad (11)$$

4. Conclusions

In this work, 3D urchin-like core–shell TiO_2@Gr (UTG) was successfully fabricated on Si/SiO_2 substrates by a simple hydrothermal combined with thermal CVD method using sodium deoxycholate (SDC) surfactant as a carbon source. The fabricated UTG samples were used as SERS substrates to detect and decompose rhodamine B (RhB) under UV irradiation. It was found that the Gr shell played an important role in the properties of the UTG substrate. The minimum detectable concentration of RhB on the UTG SERS substrate can reach 1×10^{-9} M with an enhancement factor of 1.3×10^5. The graphene acts as the electron acceptor of TiO_2 and prevents charge recombination, and provides indirect charge transfer from TiO_2 to RhB molecules. Moreover, the UTG SERS substrate can almost completely decompose RhB with a degradation rate of 0.069 min^{-1} under UV 254 nm irradiation within 80 min. The photocatalytic degradation mechanism for the UTGs towards RhB was also presented in detail. The results show that the UTG SERS substrates can be further employed for detecting substances and degrading hazardous pollutants.

Author contributions

Nguyen Thi Huyen: methodology, investigation, formal analysis, data curation, conceptualization. Tran Ai Suong Suong, Cao Thi Thanh, Pham Van Trinh, Nguyen Van Tu, Bui Hung Thang, Tran Van Hau: methodology, investigation, formal analysis. Pham Thanh Binh, Vu Duc Chinh, Pham Van Hai, Vu Xuan Hoa: investigation, formal analysis. Tran Van Tan: investigation, formal analysis. Phan Ngoc Minh: supervision, investigation. Hiroya Abe: supervision, investigation. Nguyen Van Chuc: writing – review & editing, writing – original draft, validation, supervision, project administration, methodology, investigation, formal analysis, conceptualization. All authors discussed and approved the paper.

Data availability

The datasets used and/or analyzed during the current study are available from the corresponding author upon reasonable request. In addition, all the data generated or analyzed during this study are included in this article.

Conflicts of interest

There are no conflicts to declare.

Acknowledgements

This work was financially supported by the Vietnam Academy of Science and Technology (VAST) under Project NCXS02.03/24-25.

References

1 J. Tong, H. Zhai, S. Zhao, L. Song, G. Wang, N. Feng, P. Tan, J. Xie and J. Pan, *J. Colloid Interface Sci.*, 2024, **653**, 285–295.
2 M. Rani, Keshu and U. Shanker, *Int. J. Environ. Sci. Technol.*, 2023, **20**, 5491–5508.
3 X. Song, J. He, M. Zhang, S. Zhang and J. Liu, *Colloids Surf. A Physicochem. Eng. Asp.*, 2024, **684**, 133116.
4 P. Butmee, A. Samphao and G. Tumcharern, *J. Hazard. Mater.*, 2022, **437**, 129344.
5 L. Tan, Y. Cao, J. Yan, K. Mao, L. Liu, X. Wang, W. Ye, R. A. Harris and H. Zhang, *Anal. Chim. Acta*, 2024, **1287**, 342047.
6 R. Ziad, S. Columbus, A. Elgamouz, K. Daoudi, A. N. Kawde, K. Ramachandran and M. Gaidi, *Spectrochim. Acta Part A Mol. Biomol. Spectrosc.*, 2023, **297**, 122701.
7 Y. Wang, M. Zhang, H. Yu, Y. Zuo, J. Gao, G. He and Z. Sun, *Appl. Catal., B*, 2019, **252**, 174–186.
8 Z. Li, K. Han, A. Zhang, T. Wang, Z. Yan, Z. Ding, Y. Shen, M. Zhang and W. Zhang, *Talanta*, 2024, **266**, 125070.
9 B. Zhao, H. Liu, L. Xia, Z. Wang and C. Zhang, *ACS Appl. Nano Mater.*, 2022, **5**, 15341–15352.
10 X. Jiang, D. Yin, M. Yang, J. Du, W. Wang, L. Zhang, L. Yang, X. Han and B. Zhao, *App. Surf. Sci.*, 2019, **487**, 938–944.
11 X. Zhang, N. Wang, R. Liu, X. Wang, Y. Zhu and J. Zhang, *Opt. Mater. Express*, 2018, **8**, 704–717.
12 M. Zhang, H. Sun, X. Chen, H. Zhou, L. Xiong, W. Chen, Z. Chen, Z. Bao and Y. Wu, *J. Alloy. Compd.*, 2021, **864**, 158189.
13 K. P. Cabral, W. Kurniawan and H. Hinode, *J. Environ. Chem. Eng.*, 2015, **3**, 2786–2796.
14 H. Li, B. Yang, B. Yu, N. Huang, L. Liu, J. Lu and X. Jiang, *App. Surf. Sci.*, 2021, **541**, 148486.
15 W. Liu, Z. Wang, W. Yan, Z. Zhao, L. Shi, L. Huang, Y. Liu, X. He and S. Cui, *Carbon*, 2023, **202**, 389–397.
16 X. Ling, L. G. Moura, M. A. Pimenta and J. Zhang, *J. Phys. Chem. C*, 2012, **116**, 25112–25118.
17 L. L. Qu, N. Wang, Y. Y. Li, D. D. Bao, G. H. Yang and H. T. Li, *J. Mater. Sci.*, 2017, **52**, 8311–8320.
18 A. R. Biris, D. Toloman, A. Popa, M. D. Lazar, G. K. Kannarpady, V. Saini, F. Watanabe, B. P. Chhetri, A. Ghosh and A. S. Biris, *Phys. E*, 2016, **81**, 326–333.
19 M. A. Fitri, M. Ota, Y. Hirota, Y. Uchida, K. Hara, D. Ino and N. Nishiyama, *Mater. Chem. Phys.*, 2017, **198**, 42–48.
20 H. Liu, Z. Chen, L. Zhang, D. Zhu, Q. Zhang, Y. Luo and X. Shao, *J. Phys. Chem. C*, 2018, **122**, 6388–6396.
21 S. Karamat, U. Khalique, A. Usman, A. Javaid and A. Oral, *Arab J. Sci. Eng.*, 2022, **47**, 7779–7788.
22 G. Lui, J. Y. Liao, A. Duan, Z. Zhang, M. Fowler and A. Yu, *J. Mater. Chem. A*, 2013, **1**, 12255.
23 X. Jiang and J. Wang, *App. Surf. Sci.*, 2023, **612**, 155849.
24 Z. Zhou, R. Yang, Y. Teng, Y. Li and M. Wei, *J. Colloid Interface Sci.*, 2023, **637**, 533–540.
25 N. G. Nair, V. G. Gandhi, K. Modi and A. Shukla, *Mater. Today Proc.*, 2024, DOI: **10.1016/j.matpr.2023.12.049**.
26 D. Heltina, D. I. Mastura, A. Amri and M. P. Sembiring, *Mater. Today Proc.*, 2023, **87**, 293–298.
27 A. B. Migdadi, Q. M. Al-Bataineh, A. A. Ahmad, H. M. Al-Khateeb and A. Telfah, *J. Alloy. Compd.*, 2024, **971**, 172794.
28 S. Wannapop and A. Somdee, *Ceram. Int.*, 2020, **46**, 25758–25765.
29 L. Xiang, X. Zhao, J. Yin and B. Fan, *J. Mater. Sci.*, 2012, **47**, 1436–1445.
30 C. Shi, M. Eqi, J. Shi, Z. Huang and H. Qi, *J. Colloid Interface Sci.*, 2023, **650**, 1736–1748.
31 A. Kumar, A. R. Madaria and C. Zhou, *J. Phys. Chem. C*, 2010, **114**, 7789.
32 M. Lv, D. Zheng, M. Ye, L. Sun, J. Xiao, W. Guo and C. Lin, *Nanoscale*, 2012, **4**, 5872–5879.
33 Y. Jiang, W. Zhao, S. Li, S. Wang, Y. Fan, F. Wang, X. Qiu, Y. Zhu, Y. Zhang, C. Long and Z. Tang, *J. Am. Chem. Soc.*, 2022, **144**, 15977–15987.
34 C. T. Thanh, N. T. Huyen, P. V. Trinh, N. V. Tu, V. T. Thu, V. C. Tu, D. N. Nhiem, P. T. Binh, N. N. Anh, V. X. Hoa, P. N. Minh, H. Abe and N. V. Chuc, *Diamond Relat. Mater.*, 2025, **152**, 111889.
35 P. N. D. Duoc, N. H. Binh, T. V. Hau, C. T. Thanh, P. V. Trinh, N. V. Tuyen, N. V. Quynh, N. V. Tu, V. D. Chinh, V. T. Thu, P. D. Thang, P. N. Minh and N. V. Chuc, *J. Hazard. Mater.*, 2020, **400**, 123185.
36 C. T. Thanh, P. N. D. Duoc, P. V. Trinh, N. T. Huyen, N. V. Tu, C. T. Anh, P. V. Hai, K. Yoshida, H. Abe and N. V. Chuc, *Mater. Lett.*, 2023, **330**, 133308.
37 S. Kumar, R. D. Kaushik, G. K. Upadhyay and L. P. Purohit, *J. Hazard. Mater.*, 2021, **406**, 124300.
38 C. T. Thanh, N. T. Huyen, V. T. Thu, P. V. Trinh, N. V. Tu, B. H. Thang, T. V. Hau, D. Tuan, M. T. Phuong, P. T. Binh, P. N. Minh, H. Abe and N. V. Chuc, *Mater. Lett.*, 2025, **386**, 138209.
39 Y. Wang, Z. Mo, P. Zhang, C. Zhang, L. Han, R. Guo, H. Gou, X. Wei and R. Hu, *Mater. Des.*, 2016, **99**, 378–388.
40 J. Wang, L. Jiang, F. Liu, M. Jia, M. Liu, J. Li and Y. Lai, *Chem. Eng. J.*, 2021, **407**, 127195.
41 L. T. Q. Ngan, D. T. Cao, C. T. Anh, K. N. Minh and L. V. Vu, *J. Electron. Mater.*, 2019, **48**, 5328–5332.
42 P. Dai, Y. Xue, X. Wang, Q. Weng, C. Zhang, X. Jiang, D. Tang, X. Wang, N. Kawamoto, Y. Ide, M. Mitome, D. Golberg and Y. Bando, *Nanoscale*, 2015, **7**, 18992–18997.
43 X. Chen, L. Zhu, Z. Ma, M. Wang, R. Zhao, Y. Zou and Y. Fan, *Nanomaterials*, 2022, **12**, 2394.
44 E. C. Le Ru, E. Blackie, M. Meyer and P. G. Etchegoin, *J. Phys. Chem. C*, 2007, **111**, 13794–13803.
45 X. Y. Wang, W. Y. Zhang, Y. J. Hu, H. Y. Song, A. Zeeshan, C. Ge and S. B. Liu, *Spectrochim. Acta, Part A*, 2024, **310**, 123932.
46 T. B. Pham, T. H. C. Hoang, V. H. Pham, V. C. Nguyen, T. V. Nguyen, D. C. Vu, V. H. Pham and H. Bui, *Sci. Rep.*, 2019, **9**, 12590.
47 X. Chong, B. Zhao, R. Li, W. Ruan and X. Yang, *Colloids Surf. A Physicochem. Eng. Asp.*, 2015, **481**, 7–19.
48 H. Y. Wu, H. C. Lin, Y. H. Liu, K. L. Chen, Y. H. Wang, Y. S. Sun and J. C. Hsu, *Molecules*, 2022, **27**, 6755.
49 S. Kumar, D. K. Lodhi and J. P. Singh, *RSC Adv.*, 2016, **6**, 45120.

50 W. Chen, W. Wang, H. Xing, W. Li, H. He, W. Li, P. K. Chu, G. Song, H. Wang and P. Li, *Surf. Interfaces*, 2023, **38**, 102808.
51 H. Zhai, C. Zhu, X. Wang, Y. Yan and H. Tang, *Front. Chem.*, 2022, **10**, 992236.
52 H. K. Chin, P. Y. Lin, J. Chen, R. Kirankumar, Z. H. Wen and S. Hsieh, *Appl. Sci.*, 2021, **11**, 4914.
53 D. Korcoban, A. E. Kandjani, V. E. Coyle and E. K. Alenezy, *App. Surf. Sci*, 2022, **578**, 151852.
54 U. Malik, D. Korcoban, S. Mehla, A. E. Kandjani, Y. M. Sabri, S. Balendhran and S. K. Bhargava, *App. Surf. Sci*, 2022, **594**, 153383.
55 S. P. Godad and S. Kamal, *Spectrochim. Acta, Part A*, 2021, **236**, 120176.
56 H. Qiu, M. Wang, M. Cao, L. Zhang, S. Ji, J. Dou, Y. Ji, S. Kou, J. Guo and Z. Yang, *App. Surf. Sci.*, 2019, **489**, 1010–1018.
57 S. Ji, S. Kou, M. Wang, H. Qiu, X. Sun, J. Dou and Z. Yang, *App. Surf. Sci.*, 2019, **489**, 1002–1009.
58 H. Qiu, M. Wang, L. Zhang, M. Cao, Z. Yang, J. Dou, S. Ji, Y. Ji, S. Kou and A. S. Bhatti, *Carbon*, 2019, **152**, 305–315.
59 W. Pan, L. Liu, Y. Liu, S. Xu, J. Zhou, A. Tang and J. Xue, *J. Environ. Chem. Eng.*, 2023, **11**, 111355.
60 G. Su, L. Liu, X. Liu, L. Zhang, J. Xue and A. Tang, *Ceram. Int.*, 2021, **47**, 5374–5387.
61 G. Su, L. Liu, Q. Kuang, X. Liu, W. Dong, M. Niu, A. Tang and J. Xue, *J. Mol. Liq.*, 2021, **335**, 116566.
62 S. Kumar, R. D. Kaushik and L. P. Purohit, *J. Colloid Interface Sci.*, 2023, **632**, 196–215.
63 S. Kumar, R. D. Kaushik and L. P. Purohit, *J. Hazard. Mater.*, 2022, **424**, 127332.
64 X. Zhang, C. Shao, X. Li, J. Miao, K. Wang, N. Lu and Y. Liu, *J. Alloy. Compd.*, 2016, **686**, 137–144.